Electronics and Electrical Engineering

AIMS Electronics and Electrical Engineering, 10(1): 1–25.
DOI: 10.3934/electreng.2026001
Received: 20 May 2025
Revised: 29 September 2025
Accepted: 13 October 2025
Published: 05 January 2026

https://www.aimspress.com/journal/ElectrEng

Research article

Towards miniature multi-bore coaxial reactors for microwave-assisted parallel liquid heating: Basis experimental research

Guennadi A. Kouzaev*

Department of Electronic Systems, Norwegian University of Science and Technology – NTNU, Trondheim, NO-7491, Norway

* **Correspondence:** Email: guennadi.kouzaev@ntnu.no; Tel: +47 97739617.

Abstract: This paper proposes a concept of miniature multi-bore coaxial reactors with potential applications in microwave-assisted combinatorial chemistry. The reactor consists of a shielded cylindrical dielectric core with multiple bores. Current-carrying wires placed several or only one bore, while others support the flowing liquids that are heated in parallel by the wire's electrical field. Initially, the design concept is confirmed through COMSOL electromagnetic numerical simulations of modes propagating in multi-bore coaxial waveguides. Experimental proofs are obtained by investigating the microwave heating of flowing ethanol, methanol, and reverse-osmosis water in a two-bore alumina eccentric coaxial waveguide, where the second channel contains an open-ended current-carrying wire. Joint analyses of temperature profiles, measured by an optical fiber sensor at three points of a PTFE liquid-filled tube installed inside a bore, and of input and reflected power curves measured by microwave meters, are performed. The results demonstrate adequate parallel heating of liquids using an open-ended wire heater, a configuration that can be extended to other multiple-bore coaxial reactors. It is expected that the proposed concept, confirmed by experiments and simulations, will find applications in multi-tube liquid heating and MW combinatorial chemistry.

Keywords: continuous-flow microwave heating systems; miniature multi-bore coaxial reactors

Abbreviations: EM: Electromagnetic; ID: Internal diameter; MW: Microwave; OD: Outer diameter; PM: Power meter; PTFE: Polytetrafluoroethylene; SMA: Super miniature type A; TEM: Transverse electromagnetic; VNA: Vector network analyzer

1. Introduction

Microwave-assisted chemistry relates to the application of electromagnetic (EM) waves to heat polar or ionic/polar liquid mixtures and initiate rapid chemical reactions [1,2]. The advantages and drawbacks of microwave (MW) reactors have been discussed in many papers [3,4]. Some of them are the significant acceleration of chemical synthesis, the decarbonization of chemical processes, the possibility of precise electronic control of microwave reactors, especially using semiconductor generators, a decrease in by-product yield, and potential for green chemistry.

Two main techniques are used in microwave-assisted chemistry. The first is batch chemistry, in which vessels containing liquids are placed in MW ovens, where reagents and solvents are heated to boiling or maintained under increased pressure [1,2]. The second type is a continuous-flow reactor [1,5–7], in which quartz or polytetrafluoroethylene (PTFE) tubes are installed in the ovens, where the flowing liquids are heated. Typically, the flow rate is set to around 1 mL/min to ensure the required residence time of the mixture in a strong MW heating field. Both techniques are limited in productivity due to MW losses; the penetration depth of EM waves in liquids is only a few centimeters at 2.45 GHz.

Several chemistry and pharmacology applications require only small amounts of products to be synthesized, such as in analytical chemistry, personalized on-demand medicine, and combinatorial pharmacology, which involves synthesizing multiple drug variants in parallel and composing libraries of experimental results with on-site spectral product analysis [8,9]. Usually, a few grams or milligrams are enough for spectrometers to determine the chemical composition without further processing. This can be realized in microfluidic form [10–12].

Combinatorial chemistry can be accelerated using ideas and hardware from MW-assisted technology [13,14]. For instance, in [15], a two-tube reactor was described in which plastic tubes were installed in parallel in an MW oven for drug manufacturing on a milligram scale. An industrial-scale multitubular drug synthesis system (1 kg/day) was described in [16], where 7-mm plastic tubes were installed in a rectangular waveguide cavity tuned by two three-stub tuners and two waveguide shortening stubs of variable length. A 2-kW MW generator fed this oven. Another design was numerically modeled in [17,18], where 2.45-GHz cylindrical resonators with multiple tubes are excited by a quarter-wavelength wire, similar to [19]. The excited resonant EM field heats the liquids in the tubes, according to EM simulations. Such waveguide multi-tube systems are bulky and require rather complex mechanical tuning at high kW levels of MW generators to achieve industrial-level yields.

Another approach consists of developing MW microcircuits, in which liquids are heated separately in each channel and chemical processors are integrated with microfluidic modules [13,14]. As far as we know, the first work in this direction was published in 2007 [20]. There, a liquid was heated below a microstrip conductor placed over a channel in the microstrip substrate. In contrast to waveguide-based solutions, microstrip heaters can be applied when small sizes are necessary because their quasi-transverse EM modes have no cutoff frequencies.

According to some experiments, MW-supported microfluidics surpasses conventionally heated reactors of the same type [21]. Unfortunately, the combination of MW integration with microfluidics techniques is still in its infancy [13,14], but it may hold promise for combinatorial chemistry, which requires the parallelization of multiple reactions.

Open waveguides, for instance microstrips, which radiate higher-power waves, are potential heaters of integrated reactors. Each reactor must then be adequately shielded, as demonstrated, for instance, in [22].

Another problem that may arise even in relatively compact systems is heat removal after a cycle of high-power MW operation. Many reactions require cooling of the product to stabilize the results, which necessitates additional energy consumption and thermal insulation measures to protect different parts of the hardware in a high-temperature environment.

More serious problems occur when each integrated reactor is heated individually by an MW oscillator. In combinatorial chemistry, hundreds or thousands of generators may be required. A system powered by one generator will need a complex network of bulky power dividers to distribute energy among the integrated reactors. In this situation, miniature reactors with MW power shared between tubes, as per the reactor design, are preferable.

As for prototypes, the waveguide systems described earlier [15–18] can be employed, where the waveguide cavity resonant field heats the liquids in the tubes. Among the promising candidates are coaxial waveguides [23,24] or shielded strip lines [22] equipped with tubes, which offer viable options for miniaturized solutions.

One of the earliest studies on coaxial reactors is [25], which considers a rotating coaxial reactor for plastic chip pyrolysis at 2.45 GHz. A disadvantage of conventional coaxial waveguides is the non-uniform electric field across the cross-section [26,27]. In [28], it was proposed to pump a liquid into trenches of the dielectric core adjacent to the waveguide shield, where the electric field is smooth; some numerical simulations were conducted to validate this concept.

In general, a coaxial waveguide filled with a liquid of complex dielectric permittivity has an input impedance that deviates from 50 Ohms. This issue can be addressed over a wide frequency band by smoothly shaping the dielectric insert and the inner conductor of the coaxial vessel, as shown in [29]. The coaxial waveguide taper was used to match the length of a coaxial waveguide to a heated catalyst with gas flow [30,31]. Conical sections were used in [32] to match a coaxial waveguide with a helically shaped dielectric channel containing a flowing liquid.

An interesting approach was presented in [33], where a glass Liebig condenser was modified for MW heating of liquids. The geometry of this reactor was pre-distorted in an air-filled condition so that, upon filling with liquid, the characteristic impedance of the glass–metal reactor returned to approximately 50 Ohms, thereby reducing reflections.

Coaxial geometry was employed in a thin-film liquid rotating reactor [34], showing promise for accelerating chemical processes. Here, a liquid moves through a submillimeter gap between the stator (outer shield) and a rotating hollow dielectric rod, which is fed by a wire carrying MW current. Acceleration is achieved through enhanced mixing of agents in the liquid and MW heating. A multiwire design for smoothing the cross-sectional distribution of the electric field was described, for instance, in [24], which also discussed the miniaturization of coaxial reactors and developed a theory describing the motion of dipolar molecules in an EM MW field within nanocoaxial geometries.

This analysis reveals those coaxial structures—closed vessels that support TEM modes—are highly versatile and promising for the further development of miniature and integrated MW reactors. In particular, they can be used for multi-bore liquid heating, as mentioned in a preprint [23]. The goal of this paper is to propose miniature multi-bore coaxial designs and to provide experimental evidence of parallel MW heating of liquids in the bores of a dielectric core via wire heating.

2. Multi-bore coaxial waveguide reactor concept

We propose modifying a miniature dielectric-filled coaxial reactor into a multi-bore configuration for parallel heating of liquids. The reactor consists of a conducting wire, a shield, and a multi-bore dielectric core. When necessary, the bores can be equipped with high-temperature plastic tubes for quick replacement, thereby avoiding contamination of the entire reactor. As is well known, multiple-tube reactors increase production volume through parallelization [5]. In combinatorial chemistry, this single reactor can support multiple continuous-flow reactions within its body.

As an example, Figure 1 shows a simplified cross-section of one of the simulated waveguides, which comprises four "liquid" bores and one central current-carrying wire (white spot) within the dielectric shielded body. The geometry of this waveguide is compatible with modern low-cost glass and ceramic technologies, allowing, for instance, 2.6 mm bores to be placed 4.2 mm from the center of a 13-mm dielectric rod.

For simulation purposes, the shield and central wire are modeled as ideal conductors, and the core is assumed to exhibit no dielectric loss, unlike ethanol, which has a large dielectric loss tangent (see Table 4). Considering a real quartz core ($\varepsilon_r = 3.76$ and $tan\,\delta = 0.0001$) and copper conductors ($\sigma = 5.59 \cdot 10^7$ Sim/m) increases the loss constant by only 0.54%. Further simulations are performed using ideal materials, ignoring these losses. This simplified model nevertheless allows for studying the main properties of modes without significant loss of accuracy.

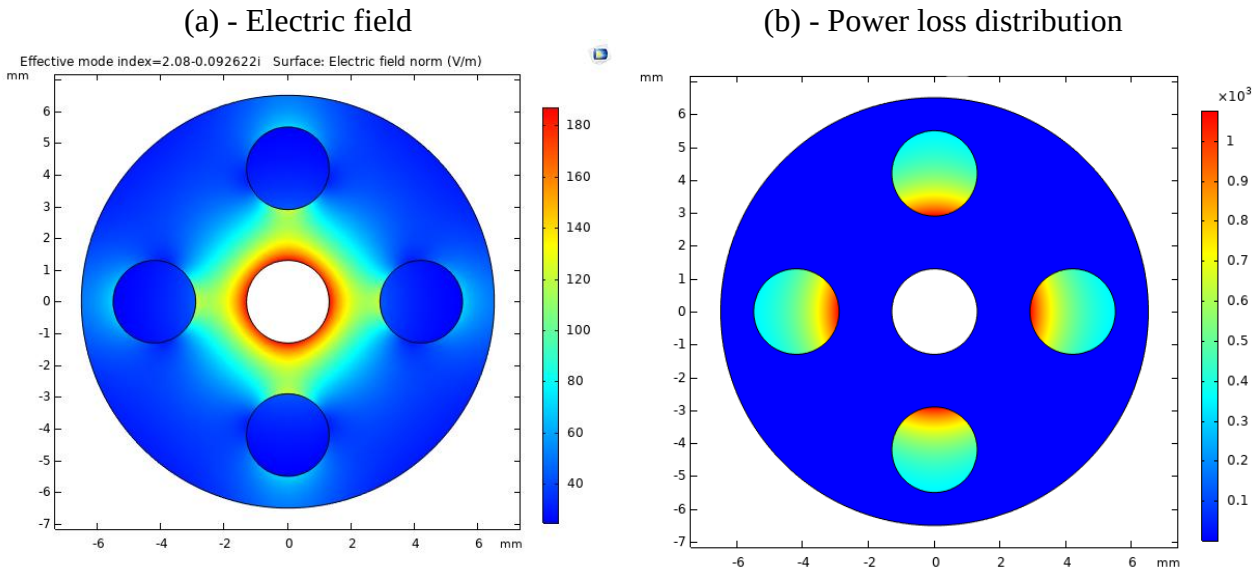

Figure 1. Ethanol-filled five-bore coaxial shielded reactor cross-section. (a) Main mode electric field distribution; (b) Power loss density (W/m^3) distribution of this mode. The white circle corresponds to the ideal conductor wire. COMSOL Multiphysics® 6.2 simulations at 2.5 GHz.

Figure 1a shows the electric field distribution of the main mode in a quartz coaxial waveguide whose four bores are filled with ethanol (Table 4). Here, the dark blue regions correspond to areas of low electric field intensity. The complex effective mode index, or normalized longitudinal propagation constant $k_z/k_{0,}$ where $k_0 = \omega/c$, and c is the velocity of light, is shown in the subtitle of the figure. Figure 1b illustrates the total power loss density distribution for this mode.

It can be observed that the electric field only slightly penetrates the liquids and is absorbed within them. These distributions in Figures 1a and 1b are not uniform due to the rapid decay of the electric field with increasing distance from the central conductor. Therefore, heating of liquids in this or similar designs should be preliminarily verified by measurements and simulations.

This investigation begins with the modeling and measurements of a two-bore shielded ceramic design (Figure 2), with the goal of applying this knowledge to multi-bores in future studies.

3. Experimental test reactor design

A tested two-bore structure (below the test reactor) is shown in Figure 2a. This device is designed to confirm the concept formulated above, comprising a dielectric (alumina) two-bore rod (Table A1, row 1), covered with a copper foil, and adhered to the reactor body with a conductive adhesive layer (Table A1, row 2). The shielding effectiveness of this foil, as per [35,36], is estimated at around 55–30 dB at frequencies from 1 to 10 GHz.

A heating open-end wire is inserted into one bore of this rod (Figure 2b), partly coated with PTFE to center the conductor and insulate the heating wire from the bore wall. This conductor is a part of a semi-rigid coaxial waveguide RG402 (www.pasternack.com), excited with an MW connector (Figure 2). The second bore is for a PTFE tube (Table A1, row 3) containing a flowing liquid.

(a)

(b)

Figure 2. (a) Test eccentric coaxial reactor with an installed exchangeable internal polymeric tube. (b) Heater with an SMA connector.

The input coaxial waveguide RG402 excites both the main and higher-order propagating modes, whose number depends on the reactor's material, geometry, and bore filling. These modes are reflected from the end of the wire and contribute to the distributed heating of the flowing liquids.

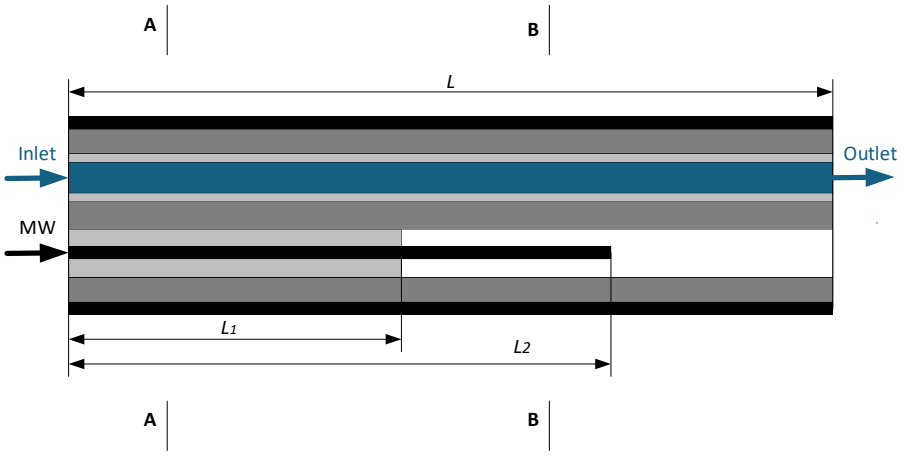

(a)

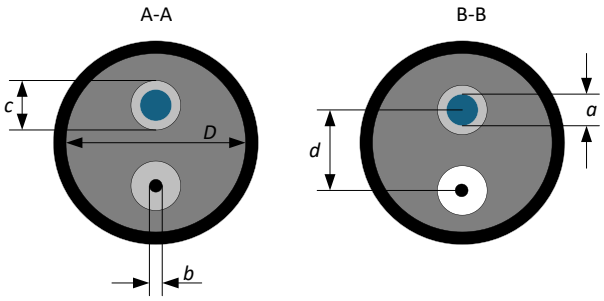

(b)

Figure 3. (a) Test reactor draft. Geometry: $L = 250$ mm, $L_1 = 67$ mm, and $L_2 = 117$ mm. (b) Cross-sections of the test eccentric coaxial reactor. Geometry: $a = 2$ mm, $b = 0.8$ mm, $c = 2.7$ mm, $d = 4.2$ mm, and $D = 10$ mm.

4. Materials and methods

4.1. Materials

The coaxial sample used in our experiments is made of alumina, although other dielectrics can also be used. All physical parameters of alumina are presented in Table 1.

Table 1. Alumina physical parameters [37].

Reactor rod (Table A1, row 1) material	Relative dielectric permittivity, ε_r	Loss tangent, $tan\,\delta$	Thermal conductivity, $\frac{W}{m \cdot K}$	Specific heat capacity, $\frac{J}{kg \cdot K}$
Alumina, Al_2O_3	9.6–9.9	0.0001–0.0004	14–30	930

Table 2. Copper foil parameters [38].

Conductive foil (Table A1, row 2)	Electric conductivity, Sim · m	Thermal conductivity, $\frac{W}{m \cdot K}$	Specific heat capacity, $\frac{J}{kg \cdot K}$
Copper, Cu	$5.9 \cdot 10^7$	401	384.4

The dielectric rod is covered with a 0.035 mm copper foil and a thin (0.025 mm) high-conductivity adhesive layer with a through-layer resistivity of 0.003 Ohm. Some copper parameters are given in Table 2.

The radiating conductor of the eccentric coaxial test reactor is made of silver-plated copper wire with a diameter of 0.91 mm. This conductor is partly covered by a PTFE layer with an outer diameter of 2.55 mm (see Figure 2). The plastic tube is made from the same material (Table A1, row 3). The parameters of the PTFE are given in Table 3.

Table 3. PTFE parameters [39].

Insulation and tube material	Relative dielectric permittivity, ε_r	Loss tangent, $tan\,\delta$	Thermal conductivity, $\frac{W}{m \cdot K}$	Specific heat capacity, $\frac{J}{kg \cdot K}$
PTFE	2.1	0.0002–0.0004	0.3	1000

Three reference liquids (ethanol, methanol, and reverse-osmosis water) were used in the experiments and simulations. Their electrical and thermal characteristics are presented in Table 4 at 25 ℃, 2.5 GHz frequency, and ambient pressure [40–45].

Table 4. Reference liquid parameters.

Liquid	Relative dielectric permittivity, ε_r	Loss tangent, $tan\,\delta$	Thermal conductivity, $\frac{W}{m \cdot K}$	Specific heat capacity, $\frac{J}{kg \cdot K}$	Boiling point, ℃
Ethanol, C_2H_5OH (Table A1, row 4)	7.10	0.86	0.167	2570	78.38
Methanol, CH_3OH (Table A1, row 5)	22.13	0.6	0.196	2530	64.7
Water, H_2O (Table A1, row 6)	78	0.134	0.598	4130	100

4.2. Methods

The primary method employed in this paper was an experimental technique used to study the frequency and thermal characteristics of the proposed design. Numerical simulations, performed using the COMSOL Multiphysics ® software tool (www.comsol.com), are for illustration purposes only.

The tested eccentric coaxial reactor sample, shown in Figures 2 and 3, was studied using a setup whose block diagram is presented in Figure 4. This setup allows generating an MW power at 2.45 GHz, measuring the input and reflected powers, and monitoring the liquid temperature inside and outside the heating area. The measurement techniques are described below. This setup includes an MW generator (1) (Table A1, row 7), whose power can be digitally adjusted in 10 W increments, and a reflectometer (2) (Table A1, row 8), which separates small portions of input and reflected signals and transmits them to power meters (PM1, Table A1, row 9, and PM2, Table A1, row 10).

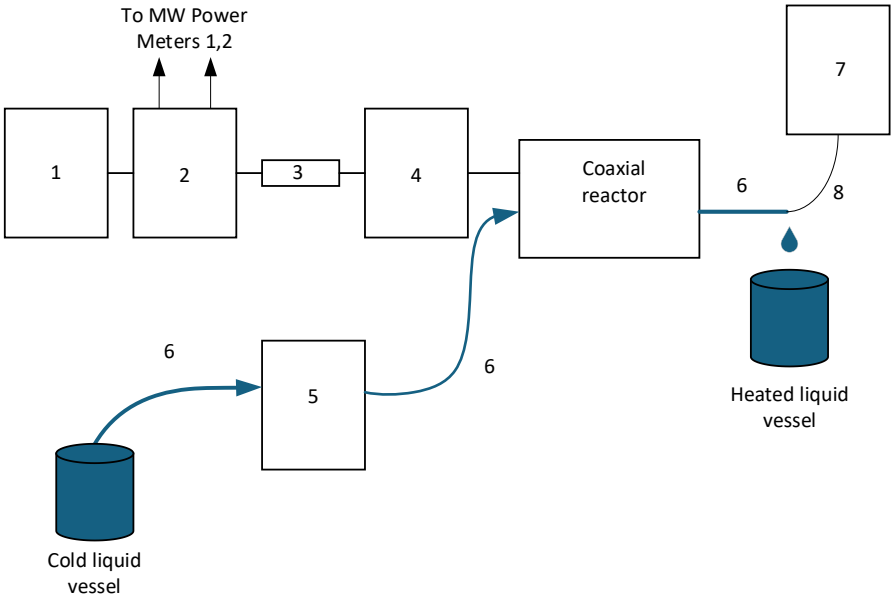

Figure 4. Block diagram of the experimental setup.

The output of the reflectometer (2) is connected through a short coaxial cable (3) (Table A1, row 11) to a three-stub impedance tuner (4) (Table A1, row 12), matching the 50-Ohm generator (1) to the complex input impedance of the tested reactor sample filled with the studied liquid. The liquid is supplied from a peristaltic pump (5) (Table A1, row 13) through Tygon tubing (6) (Table A1, row 14).

The high-power generator KU SG 2.45-250A (Table A1, row 7), manufactured by Kuhne Electronic for MW heating and chemistry, provides a maximum power output of 250 W, adjustable in 10 W increments. The generator has no option for fine-tuning this power, which can vary to some extent depending on the generator's internal properties, the inside temperature, and matching conditions. Optimal performance is achieved with large-frequency-bandwidth 50-Ohm loads. In our experiments, when matched with an impedance tuner, the generator set to 60 W output produced 57–60 W, with minor switching depending on the matching quality and bandwidth.

Experiments with high-power microwaves require additional safety. A professional MW sensor (Table A1, row 17) measures parasitic irradiation from connectors and the reactor body. Although the experimental reactor has an open end, even at a maximum input power of 60 W, the measured irradiance at a 1-cm distance was below 5 W/cm^2. This extremely low parasitic irradiation can be attributed to power absorption in lossy liquids, reflection from the wire end, and the nonpropagation of waves in a shielded dielectric rod without an internal conductor. The reactor design can also be further shortened without altering its thermal characteristics. According to strict University rules, all experiments involving toxic and flammable liquids were conducted at the department's chemical laboratory, equipped with an air-hood chamber (Figure 5), and supervised by qualified staff.

The temperature was measured with an optical fiber thermometer (7) (Table A1, row 15). A sensor, PRB-G-40, was placed inside the heated area of the reactor, transmitting the signal through an optical fiber cable (8) to the thermometer (7).

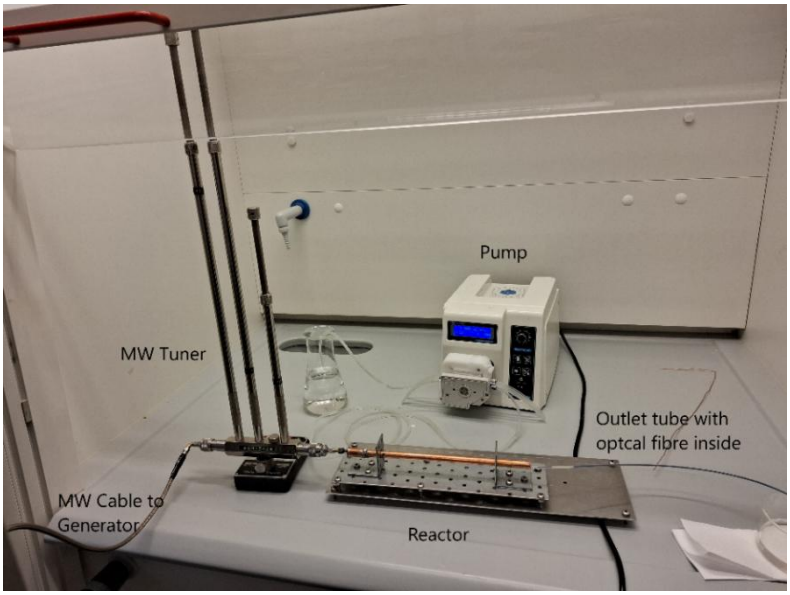

Figure 5. Eccentric coaxial reactor in an air-hood chamber of the department's chemical laboratory.

The test reactor has an open-ended inner conductor (Figures 2 and 3), which leads to increased reflection despite the lossy liquids. In this case, the use of external impedance tuners is necessary [22]. Another approach is to use reactors with self-tuning properties, as proposed in [33,46].

In this study, we employed the first method, using an external three-stub tuner (Figure 5). A block diagram of the matching setup is shown in Figure 6. It comprises a vector network analyzer (VNA) (1) (Table A1, row 16) connected via a 50-Ohm coaxial cable (2) (Table A1, row 11), and loaded by a three-stub tuner (3) (Table A1, row 14), whose output is connected to the reactor filled with the studied liquid at ambient temperature and without a probe installed.

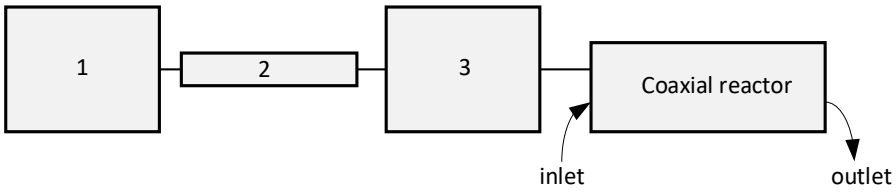

Figure 6. Matching setup.

By changing the length of the tuner stubs, the reflection coefficient S11 can be reduced to approximately –15 to –17 dB for each liquid at a generator frequency near 2.45 GHz. For example, the reflection coefficient S11 versus the frequency for the reactor filled with methanol is shown in Figure 7.

After this matching, a cable (3) (Figure 4) is connected to the reflectometer (2) output, and the heating experiments can start. However, the relative dielectric permittivity of most liquids varies with temperature, meaning that this matching is effective only under ambient conditions. As temperature increases, higher reflection levels are expected; however, the measurements indicate an acceptable level of reflection for research purposes, as shown below. Additionally, the probe installed influences the measurements due to coupling between the wire and the liquid-filled channel, which depends on both the liquid and the probe tip position. This drift in reflection can be minimized using electromechanical or electronic adaptive tuners that follow the varying input impedance of the reactor.

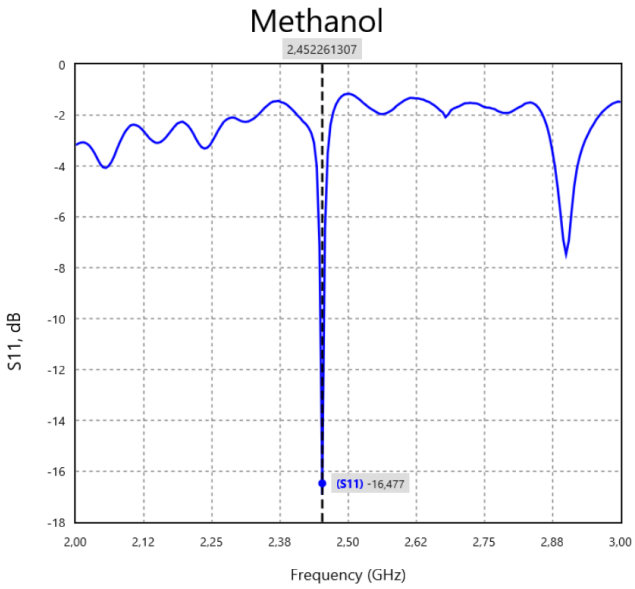

Figure 7. Reflection coefficient S11 of a tuned test reactor setup (Figures 5,6) filled with methanol.

Liquids are pumped at 1 mL/min using a Drifton peristaltic pump (Table A1, row 13, and Figure 5). Although it is a 10-roller device, slight pulsations in the liquid flow can occur. To minimize this issue, our pump is connected to the test reactor via a 1-meter Tygon tube, which is long enough to maintain smooth flow.

Temperature measurements are performed using an Osensa (www.osensa.com) probe PRB-G-40 (Table A, row 15); the probe tip is 50 mm in length and 0.65 mm in diameter. The remainder of the optical fiber cable is covered with a 1.3 mm PTFE coating. The PTFE tube has an inner diameter of 2 mm, and its insertion can disturb the electric field within the liquid and affect its thermal dynamics. Thus, all interior temperature measurements should be regarded as approximate.

5. Results

5.1. EM simulation

The multiphysics modeling of a realistic test reactor sample (Figure 2) is a complex task, even with modern software tools. Only EM numerical simulations of a simplified eccentric coaxial waveguide are performed here to avoid possible computation problems and associated inaccuracies.

For this purpose, a waveguide is used in which the thin-wall tube is excluded (Figure 8). The shield and wire conductor are represented in black, and the liquid channel is depicted in blue. It is assumed that the reactor is filled with a reference liquid at ambient temperature (25 ℃). The eigenmodes of this coaxial waveguide are calculated using the COMSOL Multiphysics® 6.2 software.

These numerical results allow estimating the distributions of the modal electric field and power loss density along the waveguide cross-section. The main mode of this waveguide was found to be quasi-TEM (transverse electromagnetic) due to the inclusion of the liquid channel. This mode can be transformed into a fully TEM mode in the case of homogeneous filling [33–47] and can be calculated semi-analytically as in an eccentric coaxial waveguide [48].

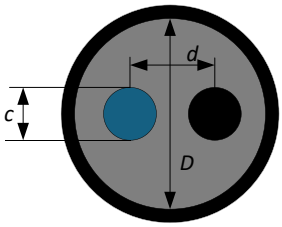

Figure 8. Simplified eccentric coaxial waveguide cross-section. Geometry: $D = 10$ mm, $d = 4.2$ mm, and $c = 3.2$ mm.

Numerical simulations indicate that this alumina (grey) waveguide, with the specified diameter, is multimodal and supports a couple of higher-order modes at a modeling frequency of 2.5 GHz. Loss of this waveguide complicates their propagation constants. Other evanescent modes also start to propagate, albeit at a decreasing rate due to loss. The propagation conditions of the second and higher-order modes can worsen if the reactor diameter and/or the relative dielectric permittivity are decreased. Additionally, the length of the wire section can be adjusted to resonate at 2.45 GHz for the main or other propagating mode. This approach allows improvement of the electric field uniformity distribution by exciting modes in a layered design. Increasing the rod diameter increases the stored reactive energy per unit length and the waveguide's quality factor, thereby improving the field uniformity along the reactor. This increases the liquid's residence time in areas with intense heating.

Below are the simulation results for the shielded eccentric coaxial waveguide filled sequentially with three reference liquids. The first two modes, along with their electric field distributions and loss power density distributions, are presented in Figures 9–14. COMSOL represents the wire in white.

Figures 9a and 9b show the electric fields of the main and first higher-order modes in a waveguide filled with ethanol. In this case, the main mode field exhibits only relatively weak concentration within the channel. At the same time, the power loss density distributions of both modes (Figures 10a,b) are comparable within this bore.

(a) - Main mode

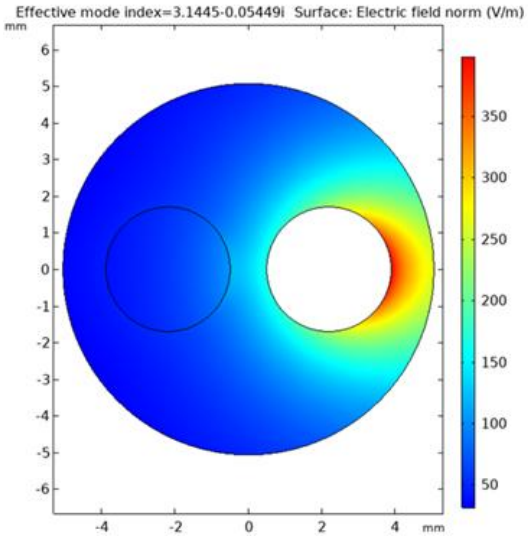

(b) - Higher-order mode

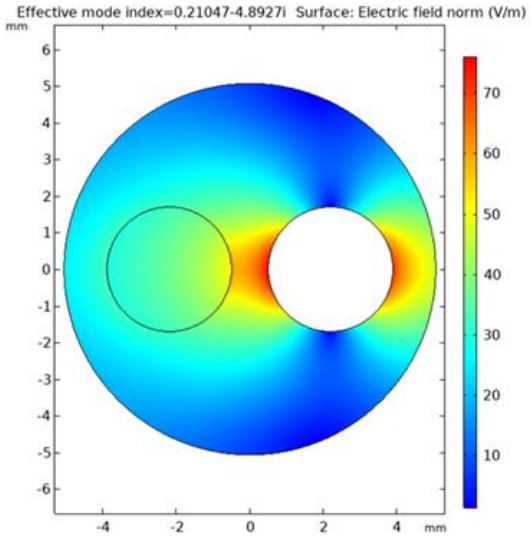

Figure 9. Electric field distribution of the first two modes in an eccentric coaxial waveguide whose first channel (left) is filled with ethanol ($f = 2.5$ GHz). An ideal conductor models the surface of the second channel and the outer conductor.

(a) - Main mode (b) – First higher-order mode

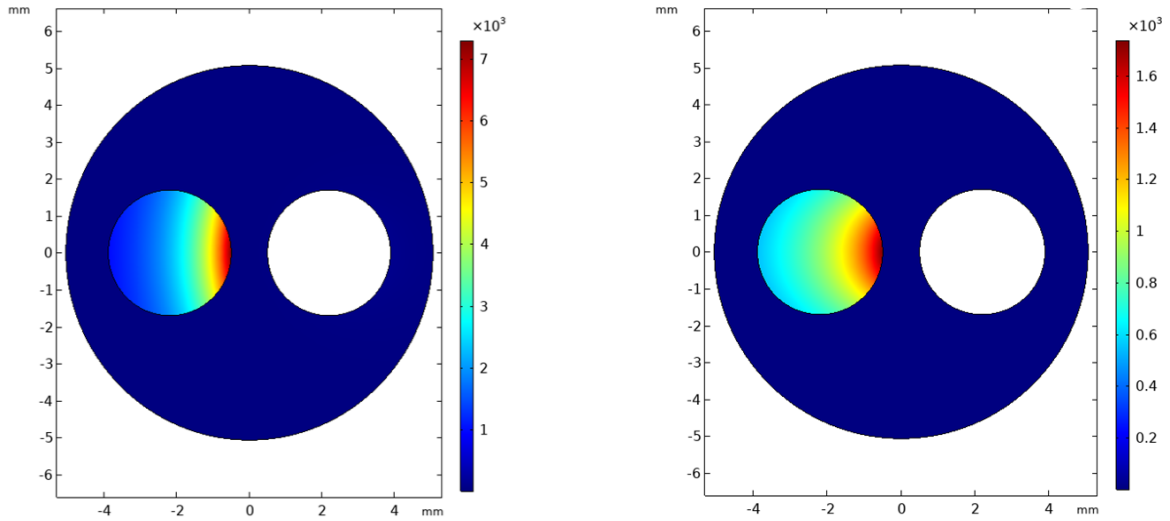

Figure 10. Power loss density (W/m^3) distribution of the first two modes in an eccentric coaxial waveguide whose first channel (left) is filled with ethanol ($f = 2.5$ GHz). An ideal conductor models the surface of the second channel and the outer conductor.

In this structure, losses occur as the liquid is heated by two modes. A distinguishing feature of the proposed heater is that the higher-order modes are excited in a distributed manner, due to coupling arising from non-homogeneous liquid permittivity along the test reactor and discontinuities in the wire channel (Figure 3). Thus, smoother temperature distributions are expected compared to those in a simple coaxial reactor [26,27].

Similarly, the electric fields and power loss density distributions are calculated in the methanol-filled reactor (Figures 11 and 12), revealing the same effect.

(a) - Main mode (b)- First higher-order mode

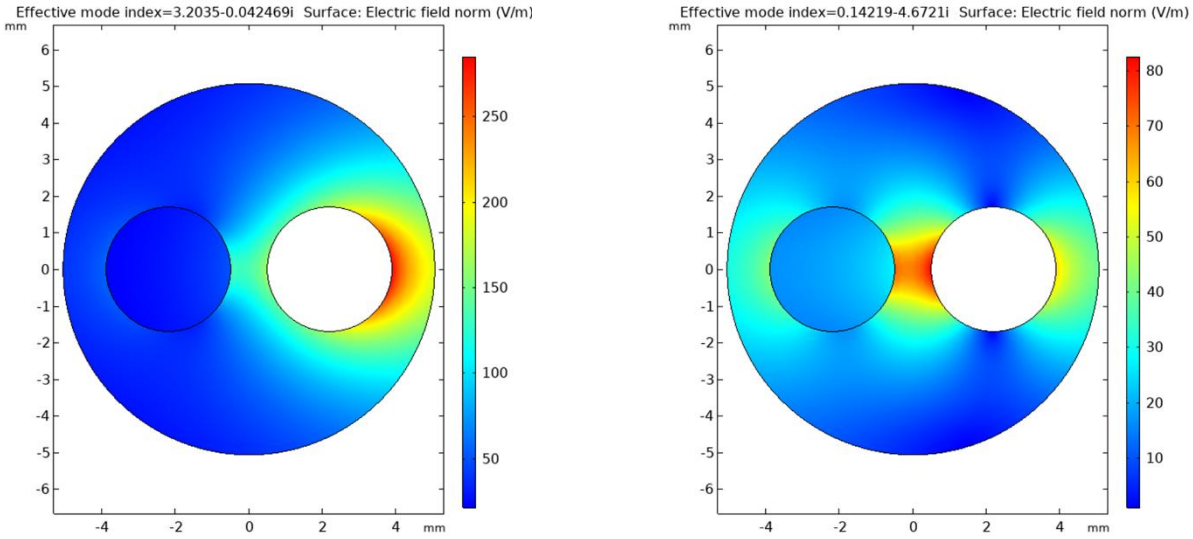

Figure 11. Electric field distribution of the first two modes in an eccentric coaxial waveguide whose first channel (left) is filled with methanol ($f = 2.5$ GHz). An ideal conductor models the surface of the second channel and the outer conductor.

(a) – Main mode (b) – First higher-order mode

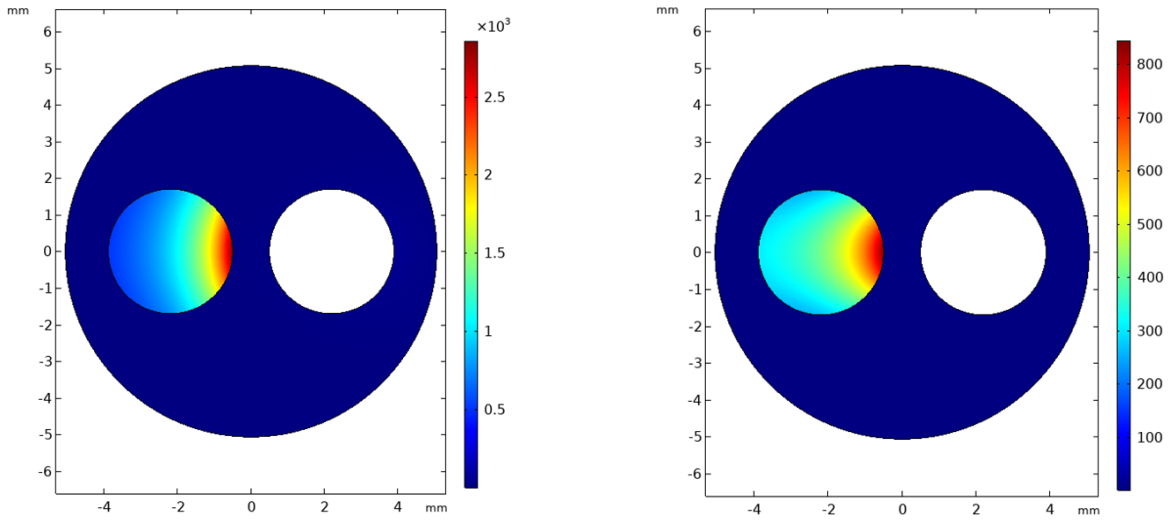

Figure 12. Power loss density (W/m^3) distribution of the first two modes in an eccentric coaxial waveguide whose first channel (left) is filled with methanol $(f = 2.5\ \text{GHz})$. An ideal conductor models the surface of the second channel and the outer conductor.

An interesting effect was found for a water-filled waveguide (Figures 13 and 14). According to different sources, the relative permittivity of this liquid is significantly higher than that of ethanol and methanol. As a result, a more concentrated EM field occurs in water-filled channels (Figures 13a and b). In particular, the higher-order mode power loss density is characterized by a homogeneous distribution within the water-filled channel (Figure 14b).

(a) - Main mode (b) - Higher-order mode

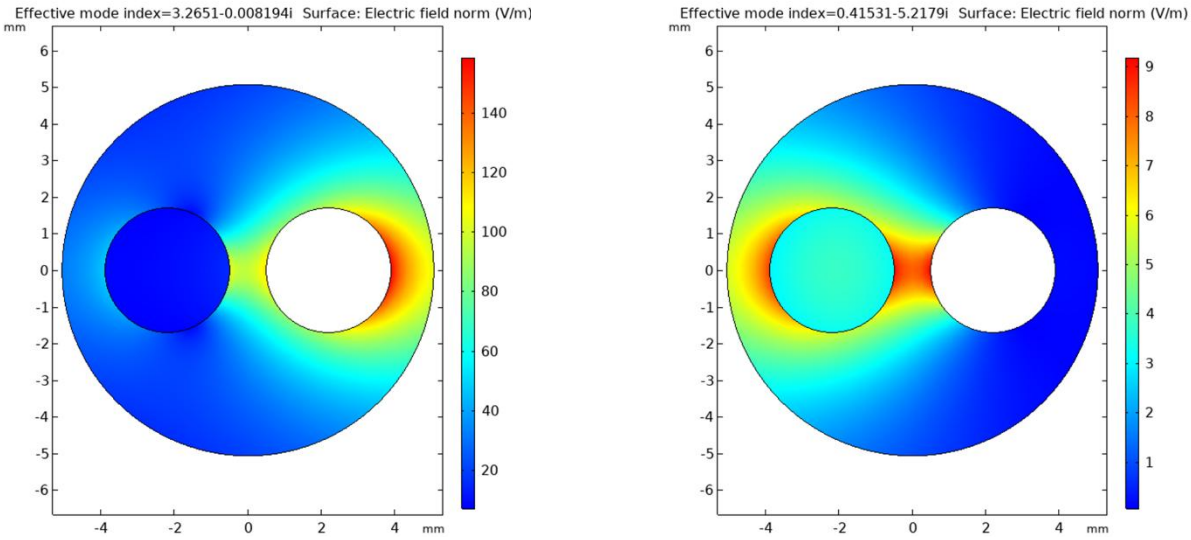

Figure 13. Electric field distribution of the first two modes in an eccentric coaxial waveguide whose first channel (left) is filled with water $(f = 2.5\ \text{GHz})$. An ideal conductor models the surface of the second channel and the outer conductor.

(a) – Main mode (b) Higher-order mode

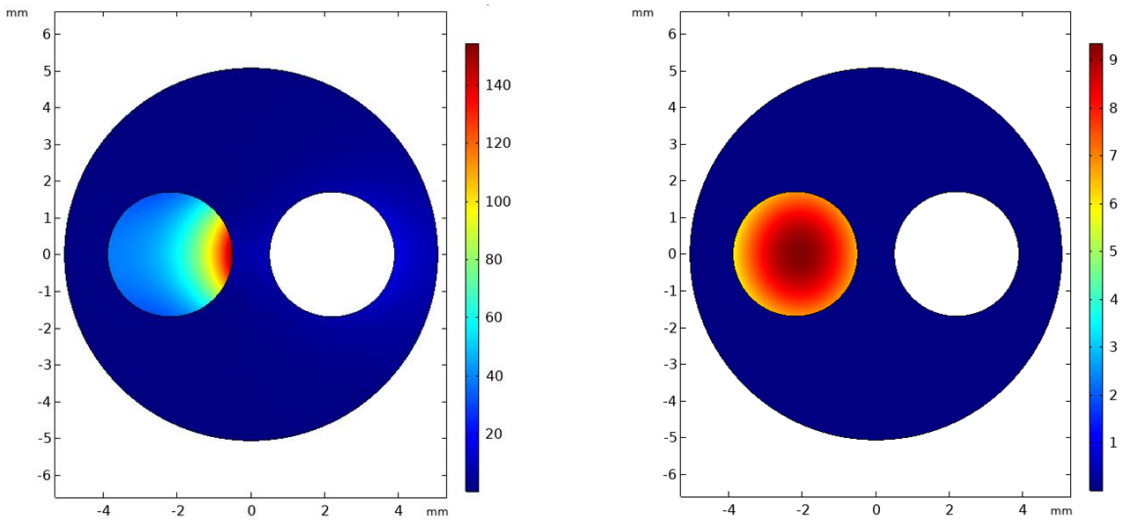

Figure 14. Power loss density (W/m^3) distribution of the first two modes in an eccentric coaxial waveguide whose first channel (left) is filled with water $(f = 2.5\ \text{GHz})$. An ideal conductor models the surface of the second channel and the outer conductor.

This allows us to preliminarily conclude that water, with a very low polar loss, can be efficiently heated in the proposed test reactor, unlike high-loss methanol and ethanol. The experiments shown in Section 5.2 below confirm this preliminary conclusion.

Simulation results for the main modes reveal a non-homogeneous distribution of the heating field, which is attributed to the coaxial design. This can lead to cross-sectional convection and to better mixing of reagents in the channel. If necessary, this non-uniformity can be reduced by decreasing the liquid channel size to submillimeter dimensions and utilizing microfluidic techniques. Otherwise, bores can be placed in regions where the electric field distribution is smoother, as done in [28].

5.2. Measurement results

All measurements begin with preliminary setup tuning (Figures 6 and 7) for each reference liquid used to fill the tested reactor sample. Then, a probe is immersed in the PTFE liquid-filled tube at a specified distance from the reactor inlet. As mentioned in Section 4, installing a probe distorts mode propagation, and the reflected power can depend on the optical fiber immersion length, liquid dynamics, and thermal conditions. This mismatching effect can be partially mitigated by individual tuning at each position along the tip end of the temperature sensor.

5.2.1. Ethanol-filled tested reactor

Figure 15a shows the temperature dependence measured 40 mm from the reactor's inlet. The reflected power $P_{\text{ref}} \leq 13\ \text{W}$ (Figure 15c) is influenced by non-ideal matching and temperature variations due to temperature reliance of ethanol's relative dielectric permittivity. The generator power $(P_{\text{in}} \approx 60\ \text{W})$ exhibits some distortion (Figure 15b), probably caused by non-ideal matching in a very narrow bandwidth, as well as long transients arising from active and passive large components.

The maximum temperature reached in this experiment was 78 ℃, slightly below the boiling point of ethanol. A smooth temperature curve indicates that no significant bubbling occurred, which is encouraging.

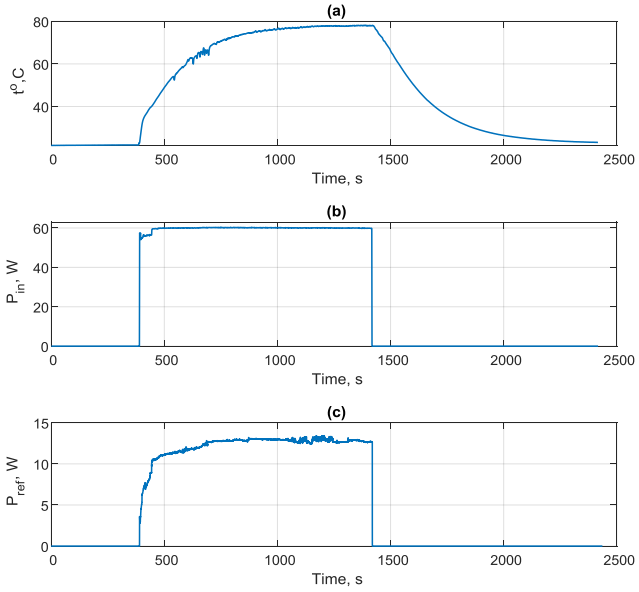

Figure 15. (a) Ethanol temperature at 40 mm from the reactor inlet. (b) Input power. (c) Reflected power.

In contrast to Figure 15, the temperature curve from Figure 16a, taken close to the end of the wire (117 mm from the inlet), exhibits some quasi-periodicity caused by bubble generation. It is taken at an input power of $P_{\text{in}} \approx 60$ W, and the reflection is below 13 W.

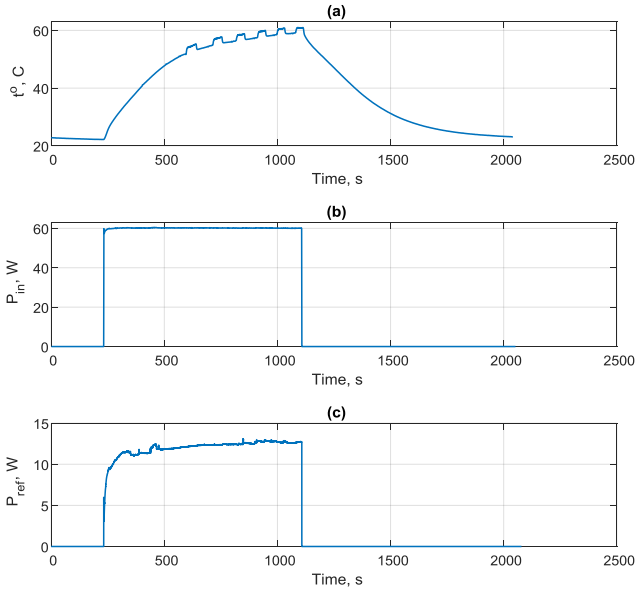

Figure 16. (a) Ethanol temperature close to the end of the heating wire (117 mm from the reactor inlet). (b) Input power. (c) Reflected power.

The maximum temperature reached was 60.94 ℃. The decrease in temperature compared to the measurements in Figure 15 was due to the interaction of ethanol with the highly thermally conductive alumina and copper shield (see Tables 1 and 2), as well as the subsequent heat evacuation through irradiation and air convection. Additionally, due to the loss of liquid and conduction, the amplitude of the electric field decreased along the heating wire. All miniature reactors operating in an

energy-economic regime require thermal insulation or use less conductive materials, such as quartz [24].

A decreased temperature value of ethanol was measured at 210 mm from the reactor inlet (Figure 17a). No large electric field exists here because the wire end is significantly distant from this point. Heat is slightly removed from the tube's ethanol due to the above-described mechanisms, and only occasional bubbling raised the temperature from below 30 ℃ to 38 ℃. The applied power was around 60 W (Figure 17b), and the reflected, slightly oscillating power level was approximately 13 W (Figure 17c).

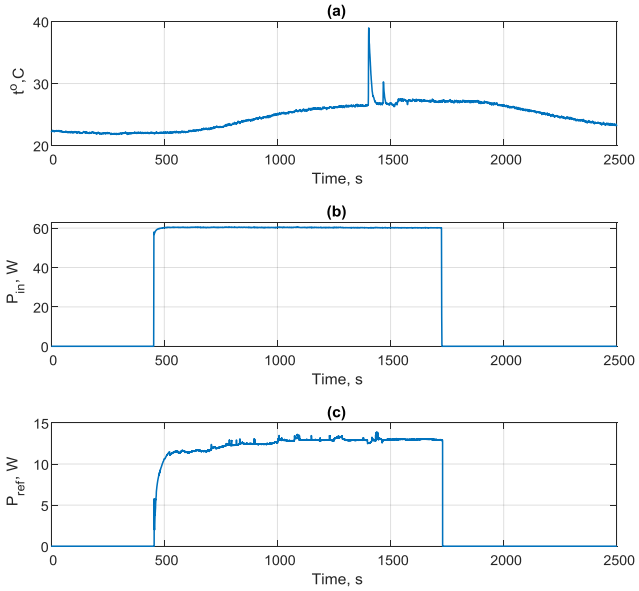

Figure 17. (a) Ethanol temperature at 210 mm from the reactor inlet. (b) Input power. (c) Reflected power.

5.2.2. Methanol-filled reactor

Measurements with methanol at the inlet of the reactor (40 mm) are shown in Figure 18. Here, with a power of around 58 W (Figure 18b), the maximum temperature was 65.62 ℃, slightly above the boiling point. The maximal reflection power reached at the end of the heating process was around 12 W.

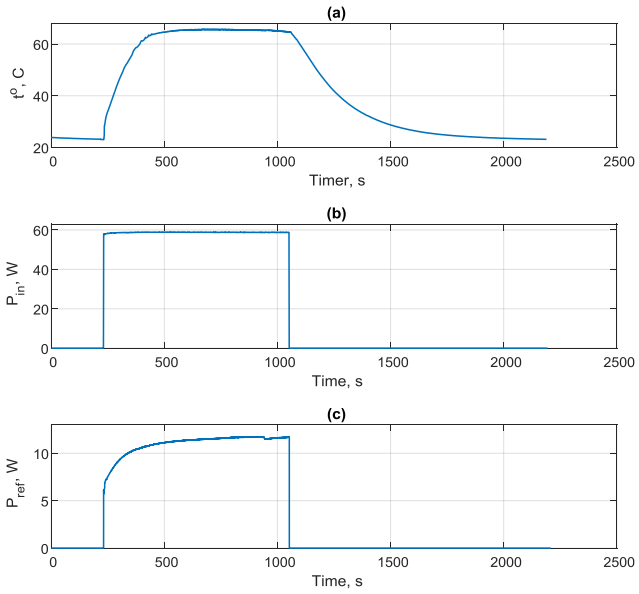

Figure 18. (a) Methanol temperature at 40 mm from the reactor inlet. (b) Input power. (c) Reflected power.

Figure 19 shows the measurements of temperature (a), input power (b), and reflected power (c) when the sensor tip is positioned at the end of the wire of the eccentric coaxial waveguide filled with methanol.

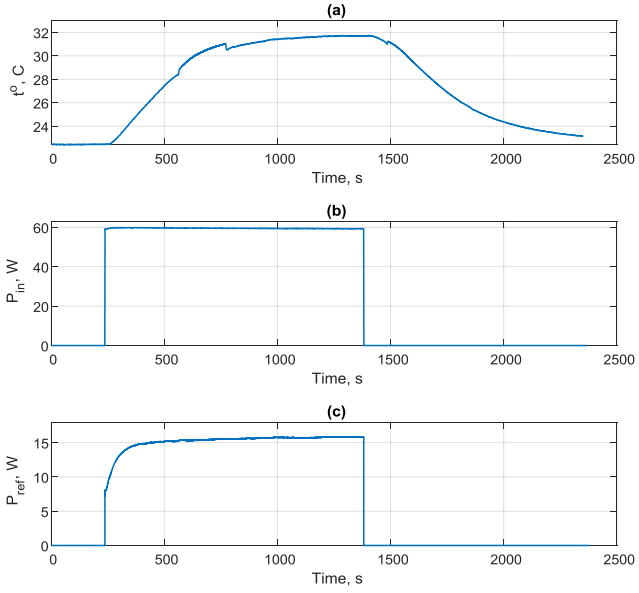

Figure 19. (a) Methanol temperature close to the end of the heating wire (117 mm from the reactor inlet). (b) Input power. (c) Reflected power.

Near the end of the reactor, the temperature further decreases further to 27 ℃ (Figure 20a). This temperature drop is delayed relative to the switching-off time of the input power (Figure 20b) due to the inertia of thermal processes in the reactor. The maximal reflected power (Figure 20c) is below 16 W at an input power of approximately 60 W.

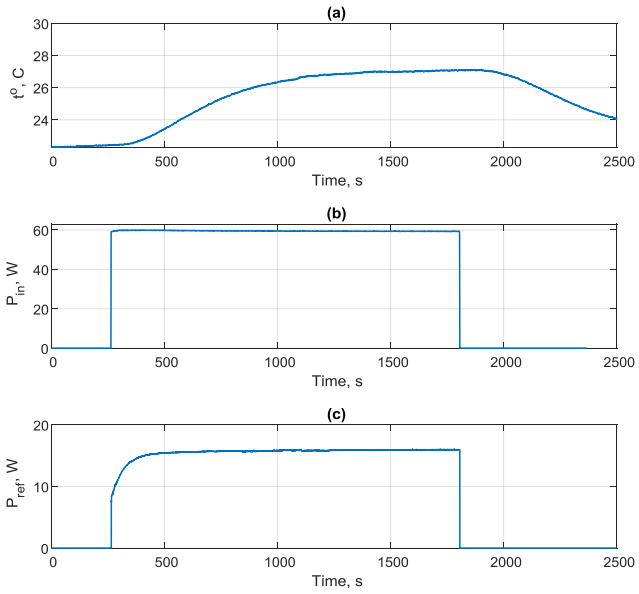

Figure 20. (a) Methanol temperature at 210 mm from the reactor inlet. (b) Input power. (c) Reflected power.

5.2.3. Water-filled reactor

The measurements with water near the reactor inlet (40 mm) are shown in Figure 21.

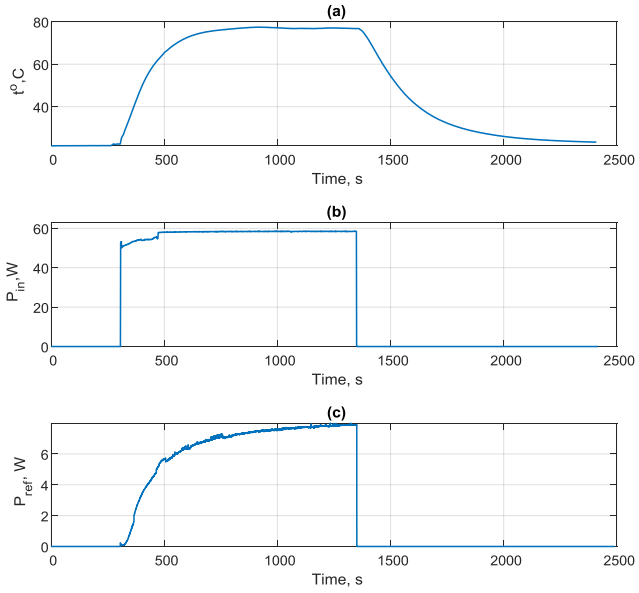

Figure 21. (a) Water temperature at 40 mm from the reactor inlet. (b) Input power. (c) Reflected power.

Water heating generally requires more power due to its low loss factor (approximately 0.137) and large heat capacity, compared to the above-studied liquids (Table 4). Besides, water's dielectric parameters vary rapidly with temperature [41]. Nevertheless, in our test reactor, heating was relatively fast, and the temperature exceeded 77 ℃ (Figure 21a) at an applied input power of approximately 58 W (Figure 21b). The maximal reflected power (Figure 21c) was around 8 W. Such relatively fast water

heating is explained by a minor reflection and distributed excitation of the first higher-order mode with its uniform loss power distribution inside the liquid bore (Figure 14b).

At the end of the heating wire (Figure 22), where the MW field still exists, the maximum temperature was around 58 ℃ (Figure 22a), with an applied power of around 58 W (Figure 22b) and a reflected power over 7 W (Figure 22c). This temperature increase is slower than in Figure 20a, and there are delays in temperature drop at power switching off.

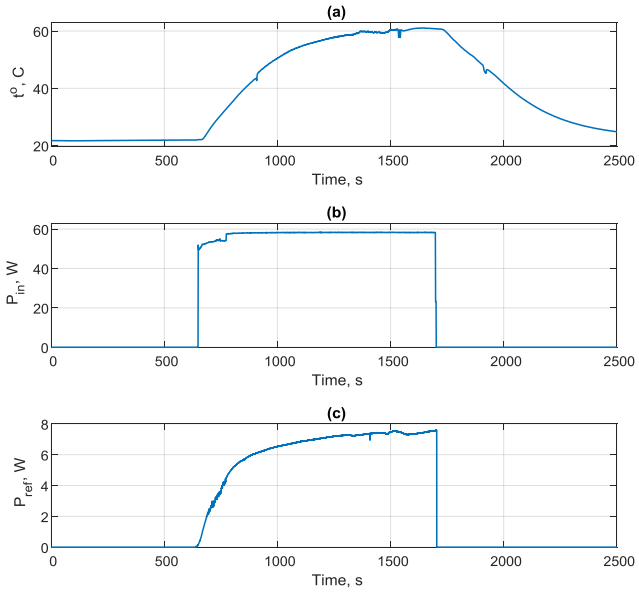

Figure 22. (a) Water temperature close to the end of the heating wire (117 mm from the reactor inlet). (b) Input power. (c) Reflected power.

As with ethanol and methanol, water measurements near the end of the reactor are shown in Figure 23.

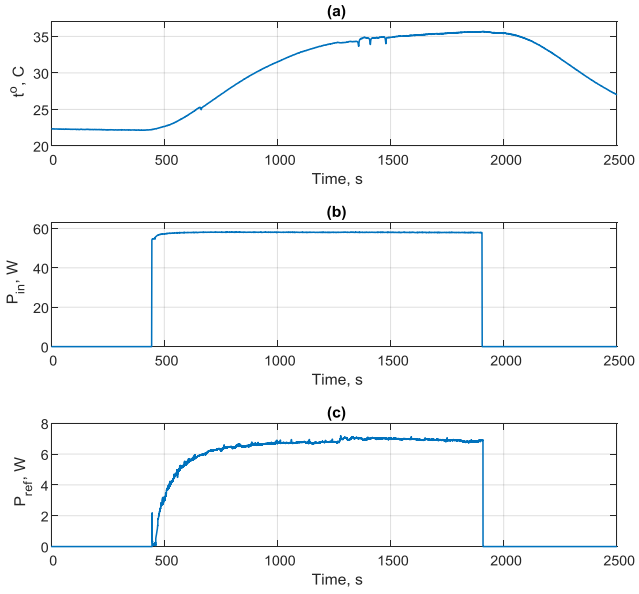

Figure 23. (a) Water temperature at 210 mm from the reactor inlet. (b) Input power. (c) Reflected power.

It is observed that water temperature increases slowly to a maximum of over 35 ℃ (Figure 23a) at an input power of 58 W (Figure 23b), with a reflected power of approximately 7 W (Figure 23c) at the end of the heating process.

6. Discussion

This paper proposes a concept for multi-bore coaxial reactors for parallel microwave heating of liquids. The current-carrying wire occupies one channel, while lossy liquids fill the others.

Initially, this idea was explored through EM simulations of electric field and power loss density distributions across the cross-sections of multi-bore coaxial waveguides. It was found that the field concentration and uniformity depend on the geometry of the waveguide and the filling liquids.

For experimental validation, a two-bore structure comprising a low-cost alumina rod, 250 mm in length, was chosen. The rod was covered in a laboratory environment with a copper foil. One channel accommodated a silver-plated copper wire connected to an MW generator, while the other housed a reference liquid flowing inside a thin-walled PTFE tube.

Considering the asymmetry of this test structure and the relatively large millimeter-scale diameter of the liquid channel, the experimentally studied geometry represents a worst-case scenario for field uniformity within this eccentric coaxial structure. Additionally, the reactor material and length have not been optimized to meet specific thermophysical parameters, thereby improving the thermal characteristics. Despite these limitations, preliminary EM simulations showed penetration of the EM field into the liquid-filled channels.

Experimental studies for this test reactor were performed with flowing ethanol (1 mL/min), methanol, and reverse-osmosis water in a PTFE tube (ID = 2.3 mm). An MW generator heated them at an output power of around 60 W. Temperature was measured at three points of this structure inside the bore's PTFE tube using an optical fiber sensor. Maximum temperatures were close to the boiling points of ethanol and methanol, measured 40 mm from the reactor inlet. Water was heated up to 78 ℃ at the same location. Peculiarities of this type of measurement have been considered in the text (Section 4).

The decrease in liquid temperature with distance from the input is due to heating of the relatively large reactor body by a small volume of fluid, along with its interaction with the environment through heat irradiation and air convection. This effect can be mitigated by using a less thermally conductive dielectric core instead of alumina or by insulating the reactor body. Another mechanism is the decline of MW power due to fluid and conductor losses, which can be reduced by using a larger-diameter wire.

It was found that the increase in reflected power with temperature accounted for the dependence of the dielectric parameters of these liquids [24]. Adaptive matching devices can compensate for it. Otherwise, this effect can also be used for real-time measurements of dielectric properties, which are needed, for instance, for rough monitoring of chemical contents [49].

These initial experiments with this test structure confirm the possibility of heating fluids using an MW current applied in an adjacent bore. Adding more liquid-filled channels does not change this principle, although it requires some geometry optimization and higher applied MW power.

Further developments may include a reactor with more liquid channels fed by a single MW generator. For instance, they can be micrometric in diameter and placed at different distances from the wire. Considering the strong radial dependence of the electric field, this effect can be compensated by an individual pumping rate for each bore if an equal temperature is required for all channels.

The reactor can be scaled up, similarly to the idea we published in 2015 [24], where a multi-conductor coaxial waveguide reactor was proposed with a smoother electric-field distribution

across the reactor's cross-section. The longitudinal penetration depth can be increased by increasing the reactor diameter, resulting in a stronger reactive energy component of the heating field and larger Q-factors for these reactors. For low-power applications, our coaxial design can be implemented in a planar form as a printed configuration, with microbores surrounding a strip conductor.

This concept, confirmed by experiments and simulations, has potential applications in multi-tube liquid heating and MW combinatorial chemistry.

Use of Generative-AI tools declaration

The author declares that he has not used Artificial Intelligence (AI) tools in the creation of this article

Acknowledgments

The author thanks the Faculty of Information Technology and Electrical Engineering (NTNU) for the sabbatical research grant in 2025. He thanks Dr. S. Pettersen for his help in the chemical laboratory.

Conflict of Interest

The author declares no conflict of interest.

References

1. *Microwaves in Organic Synthesis* (2006) A Loupy, Ed.; Wiley-VCH, Weinheim.
2. Kappe C, Stadler A, Dallinger D (2012) *Microwaves in Organic and Medicinal Chemistry*, Wiley-VCH, Weinheim. https://doi.org/10.1002/9783527647828
3. Tiwari S, Talreja S (2022) Green chemistry and microwave irradiation technique: A review. *J Pharm Res Int* 34: 74–79. https://doi.org/10.9734/jpri/2022/v34i39A36240
4. Rana K, Rana S (2014) Microwave reactors: A brief review on their fundamental aspects and applications. *Open Access Library J* 21: e686. https://doi.org/10.4236/oalib.1100686
5. Estel L, Poux M, Benamara M, Polaert I (2017) Continuous flow-microwave reactor: Where are we? *Chem Eng Proc: Process Intensification* 117: 56–64. https://doi.org/10.1016/j.cep.2016.09.022
6. Comer E, Organ M (2005) A microreactor for microwave-assisted capillary (continuous flow) organic synthesis. *J Am Chem Soc* 127: 8160–8167. https://doi.org/10.1016/j.cep.2016.09.022
7. Öhrngren P , Fardost A, Russo F, Schanche JS, Fagrell M, Larhed M (2012) Evaluation of a nonresonant microwave applicator for continuous flow chemistry applications. *Org Proc Res Dev* 16: 1053–1063. https://doi.org/10.1021/op300003b
8. Talreja S, Tiwari S (2024) From one to millions: The revolution of combinatorial chemistry. *J An Techn Res* 6: 36–42. https://doi.org/10.26502/jatr.43
9. Rasheed A, Farhat R (2013) Combinatorial chemistry: a review. *Int J Pharm Sci Res* 4: 2502–2516. https://doi.org/10.13040/IJPSR.0975-8232.4(7).2502-16
10. Parhizkar M, Tsaoulidis D (2023) Microfluidics for drug discovery and development. Chpt. 7. *In Emerging Drug Delivery and Biomedical Engineering Technologies*, 1st ed.; Lamprou, D., Ed., CRC Press, 1–8. https://doi.org/10.1201/9781003224464

11. Salley D, Manzano J, Kitson P, Cronin L (2023) Robotic modules for the programmable chemputation of molecules and materials. *ACS Central Science* 9: 1525–1527. https://doi.org/10.1021/acscentsci.3c00304
12. Greiner R, Allerdissen M, Voigt A, Richter A (2012) Fluidic microchemomechanical integrated circuits processing chemical information. *Lab Chip* 12: 5034–5044. https://doi.org/10.1039/c2lc40617a
13. Jasinska L, Malecha K (2021) Microfluidic modules integrated with microwave components—overview of applications from the perspective of different manufacturing technologies. *Sensors* 21: 1710. https://doi.org/10.3390/s21051710
14. Sun CM (2025) Combinatorial synthesis of small molecule libraries by microwave technology, In: *Frontiers in Medicinal Chemistry*, Co-eds: Rahman A., Reitz A.B.; Bentham Sci., 2: 485–510. https://doi.org/10.2174/9781608052059105020104 85
15. Comer E, Organ M (2005) A microcapillary system for simultaneous, parallel-microwave-assisted synthesis. *Chem Eur J* 11: 7223–7227. https://doi.org/10.1002/chem.200500820
16. Patil N, Benaskar F, Rebrov E, Meuldijk J, Hulshof L, Hessel V, Schouten J (2012) Continuous multitubular millireactor with a Cu thin film for microwave-assisted fine-chemical synthesis. *Ind Eng Chem Res* 51: 14344–14354. https://doi.org/10.1021/ie300754z
17. Fanti A, Casu S, Desogus F, Djuric N, Mazzarella G (2016) Design and optimization of a microwave irradiated and resonant continuous biochemical reactor. *Radio Sci* 51: 1199–1212. https://doi.org/10.1002/2016RS006018
18. Desogus F, Carta R (2019) Design of a chemical reactor under microwave irradiation in resonance conditions. *Thermal Sci* 23: 61–72. https://doi.org/10.2298/TSCI161130173D
19. Longo I, Gentili GB, Cerretelli M, Tosoratti N (2003) A coaxial antenna with miniaturized choke for minimally invasive interstitial heating. *IEEE Trans Biomed Eng* 50: 82–88. https://doi.org/10.1109/TBME.2002.807320
20. Shah J, Sundaresan S, Geist J, Reyes D, Booth J, Rao M, et al. (2007) Microwave dielectric heating of fluids in an integrated microfluidic device. *J Micromech Microeng* 17: 2224–2230. https://doi.org/10.5772/53881
21. Hur D, Say M, Diltemiz S, Duman F, Ersöz A, Say R (2018) 3D micropatterned all-flexible microfluidic platform for microwave-assisted flow organic synthesis. *ChemPlusChem* 83: 42–46. https://doi.org/10.1002/cplu.201700440
22. Kapranov S, Kouzaev G (2017) Models of water, methanol, and ethanol and their applications in the design of miniature microwave heating reactors. *Int J Thermal Sci* 122: 53–73. https://doi.org/10.1016/j.ijthermalsci.2017.08.007
23. Kouzaev G (2025) Parallel microwave-assisted heating in multi-bore coaxial reactors. *TechRxiv*, 1–3. https://doi.org/10.36227/techrxiv.174803702.26670533/v1
24. Kouzaev G (2024) *Applications of Advanced Electromagnetics. Microwave Components and Systems*, 2nd ed., Springer Nature, Switzerland. https://doi.org/10.1007/978-3-031-73892-0
25. Khaghanikavkani E, Farid M, Holdern J, Williamson A (2013) Microwave pyrolysis of plastics. *J Chem En Proc Technol* 4: 1000150. https://doi.org/10.4172/2157-7048.1000150
26. Kapranov S, Kouzaev G (2019) Study of microwave heating of reference liquids in a coaxial waveguide reactor using the experimental, semi-analytical, and numerical means. *Int J Thermal Sci* 140: 505–520. https://doi.org/10.1016/j.ijthermalsci.2019.03.023

27. Kouzaev G, Kapranov S (2020) Microwave coaxial reactors for on-demand chemistry. *TechRxiv Preprint*. https://doi.org/10.36227/techrxiv.11649678.v2
28. Sturm G, Verweij M, Stankiewicz A, Stefanis G (2014) Microwaves and microreactors: Design challenges and remedies. *Chem Eng J* 243: 147–158. https://doi.org/10.1016/j.cej.2013.12.088
29. Mitani T, Hasegawa N, Nakajima R, Shinohara N, Nozaki Y, Chikata T, et al. (2016) Development of a wideband microwave reactor with a coaxial cable. *Chem Eng J* 299: 209–216. https://doi.org/10.1016/j.cej.2016.04.064
30. Sarabi F, Ghorbani M, Stankiewicz A, Nigar H (2020) Coaxial traveling reactors: Design challenges and solutions. *Chem Eng Res Design* 153: 677–683. https://doi.org/10.1016/j.cherd.2019.11.022
31. Sarabi, Liu F, Stankiewicz A, Nigar H (2021) Reverse traveling reactor - Modeling and design considerations. *Chem Eng Sci* 246: 11682(1-7). https://doi.org/10.1016/j.ces.2021.116862
32. Duan J, Xiao W, Liu G, Yang F, Zhu H, Yang Y (2024) A high-performance microwave heating device based on a coaxial structure. *Processes* 12: 1942(1-15). https://doi.org/10.3390/pr12091942
33. Sharma G, Kouzaev G (2023) Miniature glass-metal coaxial waveguide reactors for microwave-assisted liquid heating. *AIMS Electron El Eng* 7: 100–120. https://doi.org/10.3934/electreng.2023006
34. Kouzaev G (2024) Microwave-assisted heating in a novel thin film-liquid spinning coaxial reactor. *AIMS Electron El Eng* 8: 478–497. https://doi.org/10.3934/electreng.2024023
35. Ott A (2009) *Electromagnetic Compatibility Engineering*, J. Wiley & Sons, NY. https://doi.org/10.1002/9780470508510
36. *Shielding Effectiveness of Expanded Metal Foils (EMFs)*. Dexmet Corp. 2022. Available from: https://cdn2.hubspot.net/hubfs/3798930/assets/PDF%20files/Shielding_Effectiveness_82017.pdf
37. Alumina 99.5%. Available from: https://www.microwaves101.com/encyclopedias/alumina-99-5
38. Copper. Available from: https://www.microwaves101.com/encyclopedias/copper
39. Microwave Hall of Fame. Available from: https://www.microwaves101.com/encyclopedias/ptfe
40. Gregory A, Clarke R (2012) Tables of the complex permittivity of dielectric reference liquids at frequencies up to 5 GHz. *NPL Report Mat* 23: 1–87. https://eprintspublications.npl.co.uk/2076/1/MAT23.pdf
41. Cuccurullo G, Giordano L, Viccione G (2013) Toward an improved hybrid model for simulating continuous flow microwave heating of water. In *Proc. 2013 Int. Conf. Mechanics, Fluids, Heat, Elasticity, and Electromagnetic Fields (MFHEEF)*, 182–189. Venice, Italy. http://dx.doi.org/10.13140/2.1.3966.1769
42. Navarro M (2020) Water, toluene, methanol, and ethanol under microwave irradiation: numerical simulation of the effect of the vessel's size. *J Heat Transfer* 142: 102104(1-20). https://doi.org/10.1115/1.4047512
43. Musa N, Onimisi M, Ikyumbu J (2020) Frequency and temperature dependence of ethanol using the Cole-Cole relaxation model. *Am J Con Matter Phys* 10: 44–49. http://article.sapub.org/10.5923.j.ajcmp.20201002.03.html
44. Ellison W (2007) Permittivity of pure water, at standard atmospheric pressure, over the frequency range 0-25 THz and the temperature range 0-100 ℃. *J Phys Chem Ref Data* 36: 1–18. https://doi.org/10.1063/1.2360986
45. The Engineering ToolBox. Available from: https://www.engineeringtoolbox.com

46. Kouzaev G (2025) Microwave-assisted heating in thin-film liquid spinning coaxial reactors for enhanced chemical processes. Chpt. 4, In *Chemical and Material Sciences. Developments and Innovations* 9: 62–85. http://dx.doi.org/10.9734/bpi/cmsdi/v9/3845
47. Kubiczek K (2023) Computation of the characteristic parameters of coaxial waveguides used in precision sensors. *Sensors* 23: 2324(1-11). https://doi.org/10.3390/s23042324
48. Kouzaev G (2013) *Application of Advanced Electromagnetics. Components and Systems*, 1st ed., Springer, Berlin-Heidelberg. https://doi.org/10.1007/978-3-642-30310-4_1
49. Miakawa M, Kanamori S, Hagihara K, Itagaki A, Nakamura T, Nishioka M (2021) Cylindrical resonator-type microwave heating reactor with real-time monitoring function of dielectric property applied to drying processes. *Ind Eng Chem Res* 60: 9119–9127. https://doi.org/10.1021/acs.iecr.1c00569

Appendix A

Table A1. Commercially available parts, instruments, and materials used in experiments and their main characteristics.

Item number	Notations in the text	Part name	Manufacturer/distributor	Parameters
1	Two-bore ceramic tube	Two-bore ceramic tube	*eBay*	Alumina, 10 mm diameter rod, two holes of 2.7 mm diameter
2	Conductive tape	3M 1181 copper metallic tape, 19.1 mm × 16 m	*RS Pro*	Thickness 0.035 mm, one-sided acrylic-based conductive adhesive layer
3	PTFE hose	PTFE hose	*eBay*	OD/ID = 2.5/2.3 mm
4	C_2H_5OH	Ethanol	*VWR*	99% purity
5	CH_3OH	Methanol	*VWR*	95% purity
6	H_2O	Reverse osmosis water	Prepared on-site using RIOS-50 Merck Millipore	Water resistivity 18 MOhm/cm
7	MW generator	KU SG 2.45–250 A signal generator	*Kuhne Electronic. Microwave Components*	Frequency: 2.45 GHz Output power: 0–250 W
8	Reflectometer	ZDP-BN 35691	*Rohde&Schwartz*	300 MHz–4.2 GHz
9	PM 1	Power meter MA24126A	*Anritsu*	10 MHz–26 GHz
10	PM 2	Power meter NRP-Z22	*Rohde&Schwartz*	10 MHz–18 GHz
11	0.5 m coaxial cable	Interconnect coaxial cables Sucoflex 104P	*Huber+Suhner*	Attenuation <0.5 dB m^{-1}
12	Three-stub tuner	-	*Weinschel Engineering*	1–4 GHz
13	Pump	Peristaltic dispensing	*Drifton*	Speed: 0.1–100

		pump LP-BT100-1F/DG-4(10)		rpm Flow rate: 0.2 μL to 500 mL Dispensing volume: 0.01 mL to 9900 mL
14	Tubing	Tygon tubing MHSL 2001	*Drifton*	OD 4.49 mm, ID 2.7 mm
15		Fiber optical temperature transmitter FTX-100-LUX+ and fiber optical sensor PRB-G-40 48883	*Osensa Innovation*	Temperature resolution 0.01 ℃
16	VNA	Network analyzer NanoVNA V2 Plus4 Pro	*HCXQS Group*	Bandwidth 50 kHz–4 GHz
17		Microwave leakage detector Voltcraft MNT-2G	*eBay*	Frequency 2.450 GHz